Shahid Chamran University of Ahvaz

Journal of

Applied and Computational Mechanics

Investigation of Visco-rheological Properties of Polymeric Fluid on Electrothermal Pumping

Nima Hedayati⊙, Abas Ramiar⊙, Kurosh Sedighi⊙

Faculty of Mechanical Engineering, Microfluidics and MEMs Lab, Babol Noshirvani University of Technology, Babol, Iran

Abstract. Electrothermal pumping is a recently trending method to force highly conductive fluids in a wide range of microfluidics applications with biological processes. Although most polymer fluids (biological and synthetic) are highly conductive exhibiting viscoelastic rheological properties that are relevant to biomedical applications, their behavior under the effect of electrothermal force has not yet been studied. To this aim, the PTT model (non-linear rheological constitutive equation) and electrothermal equations are implemented in the developed OpenFOAM solver. The effect of rheological characteristics of the fluids on the physical parameters such as velocity, elastic behavior, and vortices strength of electrothermal flow are investigated through the viscoelastic non-dimensional numbers. According to the results, electrothermal outlet velocity decreases by 726% as the retardation ratio (β number) increases from 0.2 to 0.9 and increases by 107% as the Weissenberg number raises from 0.001 to 10. Investigating all non-dimensional numbers simultaneously leads to the conclusion that higher electrothermal velocity is achieved by viscoelastic fluids with lower viscosity and higher relaxation time. This fact is useful for choosing the proper fluid for a particular application. As a practical example, 3000 ppm polyethylene oxide solution results in higher velocity in electrothermal flow compared to the 5% polyvinylpyrrolidone and 2000 ppm xanthan gum solution.

Keywords: Electrothermal, viscoelastic fluids, microfluid, polymer solution, PTT model.

1. Introduction

This Pumping is one of the essential processes in lab-on-a-chip devices. Electrokinetic micropumps generally require no external mechanical moving parts but possess a perfect frequency response and the ability to precisely deliver flow at high-pressure and low flow rates. They are therefore ideal for controlling flow in lab-on-a-chip devices because of these attributes. Typical electrokinetic pumping methods in microchannels are electroosmotic and electrothermal. Fluids with high conductivity cannot be pumped by the electroosmotic method while the electrothermal phenomenon can be employed by creating a volumetric force based on the temperature gradient and the change in fluid properties. Many biomedical applications utilize biological and synthetic polymer fluids, which are often highly conductive and viscoelastic. Therefore, electrothermal micropumps are recommended for pumping the fluids in microfluidic biological applications.

Many researchers have focused their studies on electrothermal and electrokinetic phenomena [1-3]. The study of Ramos et al. [4] in 1998 was among the first articles to examine this phenomenon systematically. They used linear approximations to solve the disturbance part of the equations for the first time.

According to Green et al. [5], vortices created in the electrothermal phenomenon are numerically and experimentally analyzed when an external light source is present. In the beginning, a source of light emitted uniform light, by which, the velocity in the microchannel reached 80 $\mu m/s$ while the applied frequency was equal to one Megahertz. The fluid velocity in the microchannel reached 15 $\mu m/s$ when the frequency was increased to 5 MHz.

A numerical and experimental study of alternating current electrothermal flow was carried out by Sigurdson et al. [6]. The results of experimental tests of alternating current electrokinetics have shown that electrothermal forces are more important than electroosmotic forces for electrolytes with high conductivity (0.66 S/m), which are often used in biological assays. Simulations show that an RMS voltage of 5 volts creates 2.9 Kelvin thermal differences, which creates a velocity of about 100 $\mu m/s$.

An analytical solution for two-dimensional electrothermal flow and horizontal electrodes in KCl solutions was obtained by Gonzalez et al. [7]. An electrothermal flow model with four electrodes and an external light source was conducted. The results showed that with increasing light density, the length of the particles' paths in the vortices increases, and the fluid velocity increases with voltage squared.

The electrothermal phenomenon was investigated numerically and experimentally by Wu et al. [8]. Since temperature gradient is the main factor affecting the movement of fluid in an ACET microchannel, it was shown that the pumping capability could be altered by adding a thermal chip to the microchannel.

Du and Manochehri [9] numerically investigated the channel bed shape effect on electrothermal pumping. The results showed a U groove under a large electrode can enhance pumping capacity two to three times compared to a flat surface, and a V groove under a small electrode can enhance pumping capacity by a further two to three times. In another article, the authors investigated the effects of other parameters, such as height of microchannels and longitudinal distance [10]. According to the results, in frequencies $\omega_{cr} < \omega$ & $\omega < \omega_{cr}$ the optimal behavior in the microchannel is completely different.

Yang et al. [11] numerically and experimentally studied the reverse flow in microchannels with orthogonal electrodes. In the case of micropump applications, the orthogonal electrodes generate high-velocity microcurrents when AC signals actuate them. It has been reported that three types of fluid velocity fields can be observed in the microchannel by varying the applied signals on orthogonal electrodes. The electrokinetic processes, capacitive electrode polarization, Faraday polarization, and ACET effects can all be explained by electrokinetic processes.

The effect of frequency on the flow direction alteration in microchannels was numerically investigated by Lian et al [12]. Three different conductivities (0.002, 0.02, 0.1, (S/m)) of the fluid were considered. Results indicated that the direction of fluid flow is reversed at a frequency of 1 kHz and a conductivity of 0.02 S/m.

The numerical and experimental effects of fluid conductivity on ACET were investigated by Sin et al. [13]. A pair of hook-like electrodes of the same size was used. The numerical and experimental results demonstrated that the numerical approach agrees well with the experimental conditions for conductivities between 0.01 and 1 S/m but deviates for conductivities above 0.01 S/m. According to their study, neglecting the buoyancy force when the temperature difference in the channel was 100 degrees, causes a difference between the numerical and experimental results for high conductivities.

Du et al. [14] investigated how the geometry of the channel (triangular, trapezoidal arrangement) and the arrangement of the electrodes within the channel could improve electrothermal pumping performance. In their work, four geometries were presented with a change in triangular and trapezoidal arrangement, and electrodes were embedded in the bottom.

Zhang et al. [15] proposed a coplanar asymmetric electrode arrangement for an ACET micropump in the study. By increasing the acceptable temperature and voltage, they claimed that the pumping velocity can be increased using this method. As a result of their numerical simulation, they found that this method increased the velocity of ACET by at least 25%.

According to Hong et al. [16], the classic ACET flow model (Ramos et al. [4]) is a discrete model based on the linear perturbation method, in which the effects of temperature increase on material properties should not be neglected. Therefore, they proposed a coupled model for electrical, thermal, and hydrodynamic changes. Zhang et al. [17] modeled an ACET micropump with high operating pressure and flow rate. Due to the high probability of fluid return in low-pressure micropumps (1-100 Pa), they compensate the pressure by increasing the number of electrode pairs. By using 3840 electrode pairs, the authors achieve a flow rate of 10 $\mu l/s$ and a working pressure of 12 kPa, despite the low pressure of the microchannel. Williams et al. [18] numerically investigated the effects of the thermal chip on the Joule heat generated by the electrode. The authors demonstrated that the changes caused by the chip outweigh those caused by Joule heating. Therefore, it is possible to achieve high velocity using a thermal chip by applying a lower voltage in different electrolytes.

Stubbe et al. [19] compared active and passive electrode structures for electrothermal pumping. Thermochromic beads were used to measure the temperature. By changing the color of these beads by temperature, a specific area of the channel can be examined. DC voltage was used to increase the temperature of the electrodes, and AC voltage was used to increase the velocity of the fluid. Salari et al. [20] investigated the flow characteristics of an ACET with 64 plates. Their study aimed to investigate the effect of the number of electrode pairs on fluid flow. According to the results, increasing number of electrode pairs for high conductivity fluids (1-3 S/m) is an effective method for increasing the fluid velocity.

To increase the velocity of the ACET process, Salari et al. [21] proposed a novel concept (using ring electrode pairs in the fluid channel environment). Compared to other ACET micropumps with the same electrode dimensions, their proposed micropump provides a relatively high flow rate. In addition, the research investigated the ratio of different channel dimensions, and their numerical results showed that by choosing the appropriate ratio of the electrode dimensions to the channel dimensions, an extremely efficient ACET micropump could be achieved.

It has been demonstrated numerically by Williams and Green [22] that placing a thermal chip directly under the microchannel infrastructure does not increase the flow rate of ACET but only reduces the number of vortices from four to two if the chip is placed precisely at the distance between the electrodes.

ACET and ACEO flows were numerically investigated by Vafai et al. [23], and Hoang et al. [24] in two symmetric planar electrode arrangements. They studied the effects of the electrode size and distance, the electrical conductivity of the electrolyte, the thermal conductivity of the microchannel, and the applied AC voltage and frequency on the ACET flow. ACET flow rate is independent of applied frequency in the range of the ACEO pump (100 Hz to 100 kHz), and fluid moves in the same direction as the ACEO flow.

By considering generalized viscosity for non-Newtonian fluids, Kionti et al. [25] investigated a two-dimensional numerical study of non-Newtonian fluids in electrothermal pumping and mixing. The ACET velocity of a non-Newtonian fluid was related to the applied voltage as $u V^{(4/n)}$, where u is the fluid velocity, V is the applied voltage, and n is the power-law behavior index. Their results showed that shear-thinning non-Newtonian fluids have higher velocities than Newtonian fluids.

The effect of different configurations of electrodes in the channel bed was investigated by Shojaei et al. [26] in electrothermal flow. There was a significant improvement in the outlet velocity of the fluid when the bed with upward trapezoidal, isosceles, and acute configurations of electrodes was used, as these configurations increase the outlet velocity of the fluid by 34.4% and 33% compared to the flat bed.

In the presence pressure gradient, Park et al. [27] simulated a viscoelastic non-Newtonian fluid in electroosmotic flow. By numerical coding the non-Newtonian model of Maxwell in the finite volume method, they demonstrated that viscoelastic fluids behave significantly different than Newtonian fluids under similar conditions (pressure-driven and external electric field). Huang et al. [28] investigated non-Newtonian fluids in DCEO flow numerically and experimentally. They claimed that because of the rheological complexity of non-Newtonian fluids such as DNA and blood, there are fewer publications in this field rather than other areas. Different percentages of PEO were used as a fluid with complex rheology. Results indicated that the zeta potential of a fluid with a percentage of PEO is lower than that of a Newtonian fluid. However, changes in the percentage of PEO do not affect the zeta potential. Ko et al. [29] examined the behavior of non-Newtonian fluids in a contractile microchannel under the influence of DCEO. They used four non-Newtonian fluids: PEO, PVP, PAA, and XG. A viscoelastic fluid such as PVP or PEO has weakly shear thinning and strongly elastic characteristics, whereas PAA is a strongly shear-thinning and strongly elastic fluid and XG has strongly shear thinning and weakly elastic characteristics. Their experiments revealed that PEO and PVP fluids exhibit similar behavior to Newtonian fluids. A non-linear relationship was discovered between the fluid velocity and the voltage of the XG fluid, with vortices

created before and after contraction. They also deduced that PAA fluid behaves like a Newtonian fluid before a critical voltage but collapses after this voltage. Ji et al. [30] numerically investigated the electroosmotic flow of PAA viscoelastic fluid in a contractile channel. They used the Oldryde-B model in their research.

Electrothermal pumping attracted the attention of many researchers due to its ability to control flow at low velocity, lack of mechanical moving parts, and pump fluids with high electrical conductivity. Furthermore, biological and electrolyte-based synthetic polymer solution are categorized as viscoelastic fluids in microfluidics application. Because of their electrical conductivity, electroosmotic pumping is not possible and electrothermal pumping is recommended for this type of fluids. Due to the presence of different characteristics in the properties of viscoelastic fluids, different fluid behavior in the electrothermal flow may vary. Investigating this issue can be appropriate in selecting the proper fluid to achieve the desired goals in microfluidic pumping. To our knowledge, no previous studies have examined the electrothermal pumping of viscoelastic fluid.

2.   Governing Equations

2.1 Navier–Stokes, energy and constitutive equations

The governing equations for the unsteady flow and heat transfer of an incompressible fluid are:

$$\frac{\partial \rho}{\partial t} + \nabla.(\rho \mathbf{U}) = 0 \tag{1}$$

$$\rho\left(\frac{D\mathbf{U}}{Dt}\right) = -\nabla P + \nabla.\boldsymbol{\tau}^p + \eta_s \nabla^2 \mathbf{U} + \mathbf{F}_{ET} \tag{2}$$

$$\rho c_p\left(\frac{DT}{Dt}\right) = k\nabla^2 T + \frac{1}{2}\tilde{\tau} : \tilde{\gamma} + S \tag{3}$$

where P is the pressure field, $\mathbf{F}_{ET}$ is electrothermal force, $\mathbf{U}$ is the velocity vector, η_s is the solvent viscosity, T is the temperature field, ρ is the fluid density, η_p is the polymer viscosity, k is the fluid thermal conductivity, $\gamma = \nabla \mathbf{U} + \nabla \mathbf{U}^T$, c_p is the fluid-specific heat capacity, S is joule heating source term that is calculated as $\sigma_m \mathbf{E}_0{}^2$ and $\boldsymbol{\tau}^p$ illustrates the polymeric stress tensor calculated by solving the constitutive equation. The Phan-Thien-Tanner (PTT) model, was used to mathematically describe the behavior of a viscoelastic fluid [31]:

$$\boldsymbol{\tau} = \boldsymbol{\tau}^s + \boldsymbol{\tau}^p, \qquad \boldsymbol{\tau}^s = \eta_s \gamma \tag{4}$$

$$f\left(tr\,\boldsymbol{\tau}^p\right)\boldsymbol{\tau}^p + \lambda\left(\frac{\partial \boldsymbol{\tau}^p}{\partial t} + \boldsymbol{\tau}^{p\nabla} + \xi\left(\boldsymbol{\tau}^p \gamma + \frac{\gamma}{2}\boldsymbol{\tau}^p\right)\right) = \eta_p \gamma \tag{5}$$

$$f\left(tr\,\boldsymbol{\tau}^p\right) = \begin{cases} 1 + \dfrac{\varepsilon\lambda}{\eta_p}tr\boldsymbol{\tau}^p, & \text{linear } PTT \\[2mm] 1 + \dfrac{\varepsilon\lambda}{\eta_p}tr\boldsymbol{\tau}^p + \dfrac{1}{2}\left(1 + \dfrac{\varepsilon\lambda}{\eta_p}tr\boldsymbol{\tau}^p\right)^2, & \text{quadratic } PTT \\[2mm] \exp\left(1 + \dfrac{\varepsilon\lambda}{\eta_p}tr\boldsymbol{\tau}^p\right), & \text{exponential } PTT \end{cases} \tag{6}$$

where $\boldsymbol{\tau}^{p\nabla}$ is defined as $\boldsymbol{\tau}^{p\nabla} = (\mathbf{U}.\nabla)\boldsymbol{\tau}^p - (\nabla\mathbf{U})\boldsymbol{\tau}^p - \boldsymbol{\tau}^p(\nabla\mathbf{U})^T$. The exponential form was used in this paper, which is more accurate in predicting $\boldsymbol{\tau}^p$.

2.2 Electrical field

An electric and magnetic field can be generated by applying a potential difference between two electrodes. Due to the power production ratio, the magnetic field does not have a significant impact on microstructures. Therefore, the following equation is used to calculate the electrical potential:

$$\nabla^2 \varphi = 0$$

where φ, is electrical potential. The electric field E due to the potential difference between two electrodes in the fluid is calculated as follows according to correlation of Maxwell:

$$\mathbf{E} = -\nabla\varphi$$

2.3 Electrothermal force

Electrothermal force acting on a fluid is defined as follows [26]:

$$\mathbf{F}_{ET} = \rho_q \mathbf{E}_0 - \frac{1}{2}|\mathbf{E}_0|^2 \nabla\varepsilon_m + \frac{1}{2}\nabla\left(\eta_s \frac{\partial\varepsilon}{\partial\rho}\mathbf{E}_0{}^2\right) \tag{7}$$

where $\mathbf{E}_0$ is electrical field, ρ_q is electrical charge density, ε is electrical conductivity, the forces include the Columbic force, the dielectric force, and the electrostatic force. Since the fluid is incompressible, the electrostatic force is eliminated and the above expression will be simplified as follows [26]:

$$F_{ET} = \rho_q E_0 - \frac{1}{2}\left|E_0\right|^2 \nabla \varepsilon_m \tag{8}$$

$$\rho_q = \frac{(\sigma_m \nabla \varepsilon_m - \varepsilon_m \nabla \sigma_m).E_0}{(\sigma_m + j\omega \varepsilon_m)} \tag{9}$$

By integrating the relationship (8) and (9), the electrothermal force is created as follows:

$$F_{ET} = \left(\frac{(\sigma_m \nabla \varepsilon_m - \varepsilon_m \nabla \sigma_m).E_0}{(\sigma + j\omega \varepsilon_m)}\right) E_0 - \frac{1}{2}\left|E_0\right|^2 \nabla \varepsilon_m \tag{10}$$

There is a complex term in the force calculated from Eq. (10), as the resulting force varies with the phase of the voltage applied to the electrodes. The non-dimensioned parameters were defined as follows [32]:

$$P^* = \frac{H.P}{\eta_0 U_0}, \ t^* = \frac{tH}{U_0}, \ X^* = \frac{x}{H}, \ Y^* = \frac{Y}{H}, \ U^* = \frac{U}{U_0},$$

$$F^*_{ET} = \frac{H.F_{ET}}{U_0.\eta_0}, \ T^* = \frac{T - T_{in}}{T_w - T_{in}}, \ \tau^{p*} = \frac{\tau^p}{\eta_p U_0 / H}, \ \gamma^* = \frac{\gamma H}{U_0}, \tag{11}$$

$$\frac{\partial \rho^*}{Dt^*} + \nabla.\left(\rho^* U^*\right) = 0 \tag{12}$$

$$\frac{DU^*}{Dt^*} = -\frac{1}{Re}\nabla P^* + \frac{\beta}{Re}\nabla\tau^{p*} + \frac{1-\beta}{Re}\nabla^2\left(U^*\right) + F^*_{ET} \tag{13}$$

$$\tau^{p*} + \frac{1}{Wi}f\left(tr\left(\tau^{p*}\right)\right)\tau^{p*} = \frac{\beta}{Wi}\gamma^* - \frac{\xi}{2}\left(\gamma^*.\tau^{p*} + \tau^{p*}.\gamma^*\right) \tag{14}$$

$$\frac{DT^*}{Dt^*} = \frac{1}{Pe}\nabla.\left(\nabla T^*\right) + \frac{\beta.Br}{2Pe}\tilde{\tau}^{p*} : \tilde{\gamma}^* + \frac{(1-\beta)Br}{2Pe}\tilde{\tau}^{s*} : \tilde{\gamma}^* + S^* \tag{15}$$

where Reynolds number, elasticity number, retardation ratio, pressure coefficient, Péclet number, Brinkmen number and Wissenberg number are defined as follows:

$$El = \frac{\lambda\eta_0}{\rho H^2}, \ \beta = \frac{\eta_p}{\eta_0}, \ Re = \frac{\rho U_0 H}{\eta_0}$$

$$Pe = \frac{\rho C_p U_0 H}{k}, \ Pr = \frac{\eta_0 C_p}{k} \tag{16}$$

$$El = Wi / Re$$

$$Br = \frac{\eta_0 U_0^2}{k\left(T_w - T_{in}\right)}$$

3. Geometry, Boundary Conditions and Grid Independency

Figure 1 illustrates the geometry under investigation, featuring a fluid inlet on the left and an outlet on the right. The top and bottom of the channel act as walls, with wide and thin electrodes embedded in the channel bed. The walls and electrodes are subject to a no-slip condition, while the inlet and outlet sections have zero gradient velocity. The channel measures 750 μm in length and 100 μm in height, with electrode sizes and distances between electrode pairs of 50, 150, and 50μm, respectively. The applied voltage is 10Vpp (peak-to-pack voltage). To explore grid independence results, we varied the number of meshes to 56250, 112500, and 225000 and examined changes in the velocity profile near the outlet of the channel. After observing a difference of less than 1% between the velocity profiles obtained with the maximum mesh number, we chose 112500 as the optimal mesh number for the results presented in Fig. 2.

4. Solver Algorithm

Simulations are performed in this paper using the open-source code OpenFOAM. The isothermal viscoelasticfluidfoam solver is improved by adding energy and electrostatic equations. Additionally, the momentum equation is modified to include the electrothermal force and the joule heating source terms and also viscose dissipation term is added to the energy equation. As one of the most accurate models, the PTT model was used to describe the viscoelastic behavior of the fluid. The flowchart of numerical simulation process approach is shown in Fig. 3.
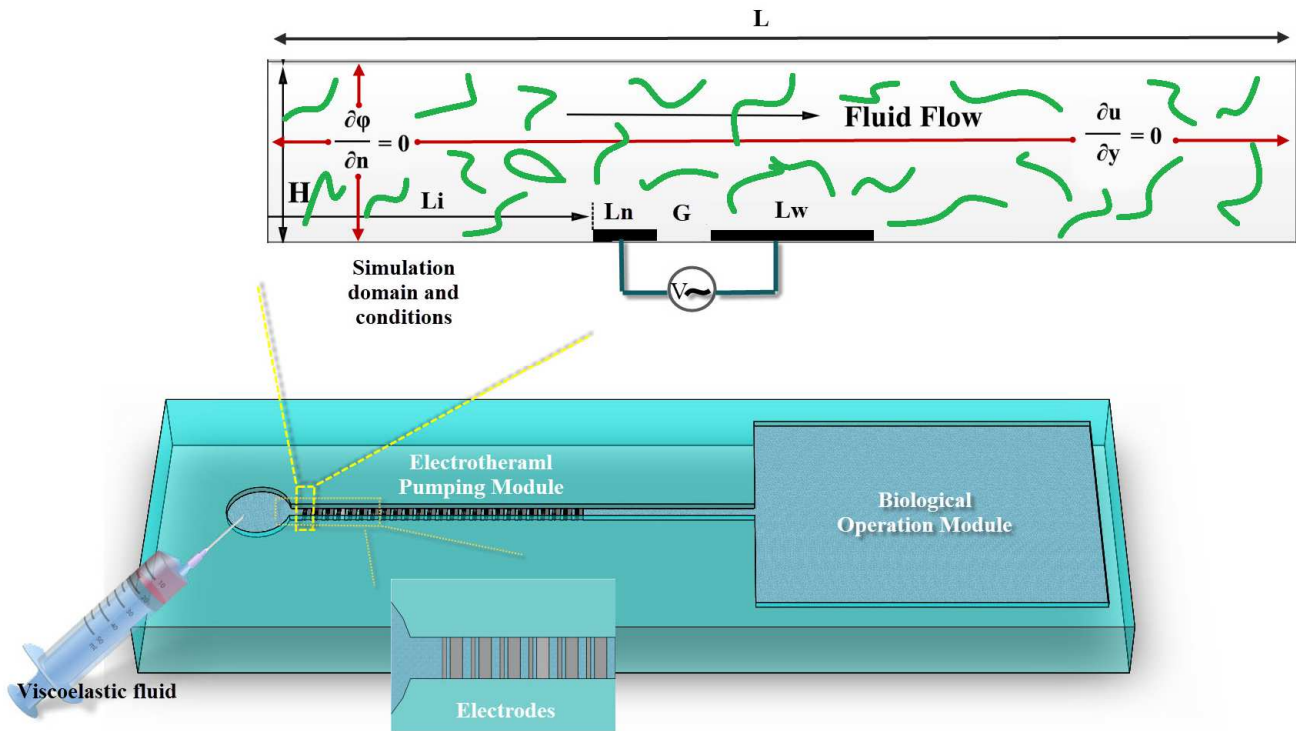
Fig. 1. Schematic of the geometry, ⌐ is schematic of Polymer macromolecule.
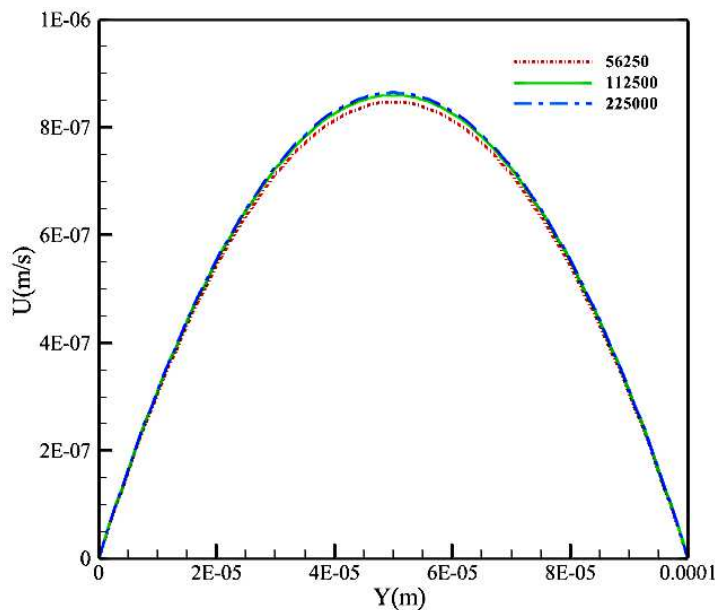
Fig. 2. Grid independency check.

5. Validation

Two validations are presented in the present study, wherein viscoelastic fluid and electrothermal flow are validated separately. Validation of the energy equation added to the Isothermal viscoelasticfluidFoam solver was performed by comparing the results with that of Minaian et al. [33] as shown in the Fig. 4. They investigated the effect of forced convective heat transfer of viscous fluid flow around a circular cylinder in low Reynolds inertial regime. In their study, they considered the geometric dimensions of the domain as ratios relative to the diameter of the circular cylinder, where this ratio was set to 20D for the fluid inlet and 35D for the width, D being the diameter of the cylinder in their work. The plot shows the local temperature parameter in the vertical line X/D=2 $(0 < Y/D < 2)$ $\beta = 0.6$, Pe $=10^4$, Br = 0, $\varepsilon = 0.1$ and $\xi = 0.01$. As a result, the absolute error in its maximum value is equal to 0.89%The velocity for fluid with different electrical conductivities was compared with experimental results (Vafaei et al. [34]) for validation of electrothermal part, in previous work of our lab [26]. There is a good agreement between the study and the experimental work of Vafai et al. [34], where the maximum error is 12% and it reduces to 2% at $\sigma = 0.178$ S/m.
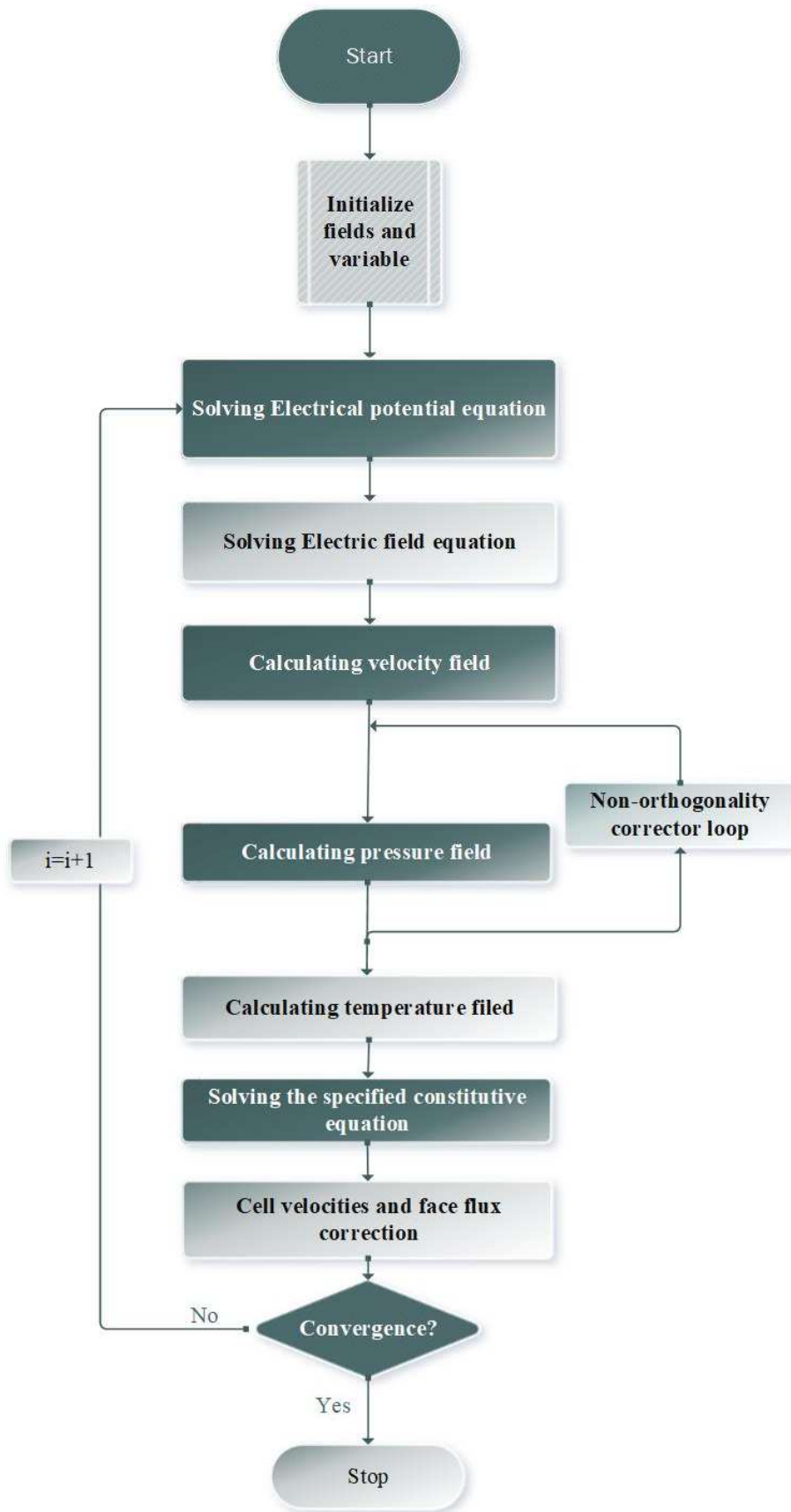
Fig. 3. Flowchart of numerical simulation process.
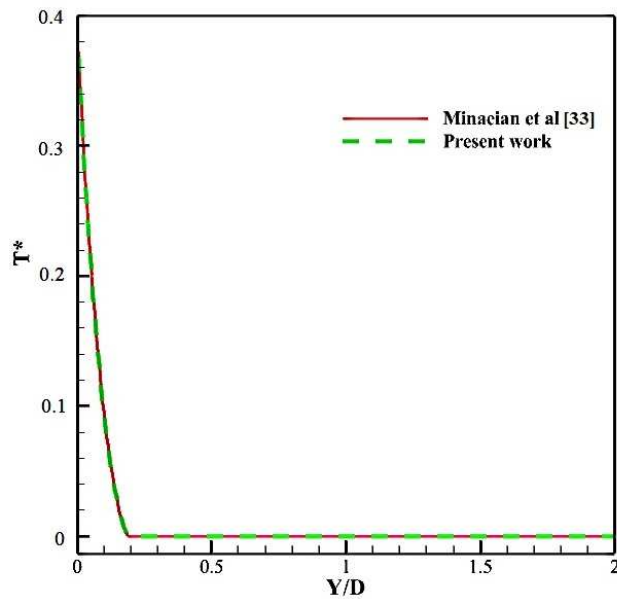
Fig. 4. Validation of the energy equation added to the viscoelastic solver with Minaian et al. [33].
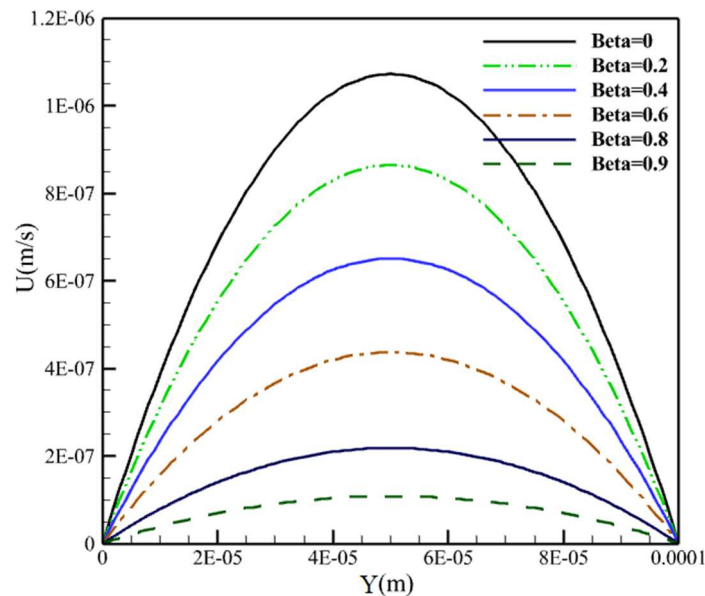
Fig. 5. Effect of dimensionless number β on the electrothermal outlet velocity.

6. Results and Discussions

Figure 5 illustrates the effect of the dimensionless number β on the electrothermal velocity in the channel outlet section. Since the β number for viscoelastic fluids varies from 0 to less than 1, a range between 0 and 0.9 have been selected with a step of 0.2 from the beginning to the end of the interval. The fluid velocity profile is a parabola illustrating the laminar flow at the microchannel outlet. Since the β number indicates the relationship between the viscosity of the polymer and the viscosity of the solvent, an increase in this number results in a higher concentration of the polymer in the solution or the presence of a polymer with higher viscosity dissolved in the solvent. As a result, the fluid velocity decreases with the increase of the β number. As indicated in Fig. 6-a, the amount of velocity for $\beta = 0.2$ is 8.26 times the value for $\beta = 0.9$, and the slop of the electrothermal velocity reduction is linear. Figure 6-b illustrates the ratio of shear rate at cross-section 1, which is at the midpoint of the gap between the electrode pairs (X = 3.25e-04 m), to the shear rate at cross-section 2 at the microchannel outlet (X = 7e-04 m). Based on the figure, as the beta value increases, the ratio of shear rate between the electrode region (X1) and the microchannel outlet (X2) becomes greater. This indicates that due to the increase in the viscosity of the viscoelastic fluid, the transfer of electrothermal force to the fluid decreases by moving from the electrode region to outside of this region.

Unlike the Newtonian fluid, the stress tensor in a viscoelastic fluid can have a diagonal component, which is the normal stress, as well as an off-diagonal component, the shear stress, which even occurs in a two-dimensional flow with a shear flow. An examination of these normal stresses and the normal stress differences can explain many of the surprising phenomena observed in the flow of complex fluids, particularly viscoelastic fluids [32].
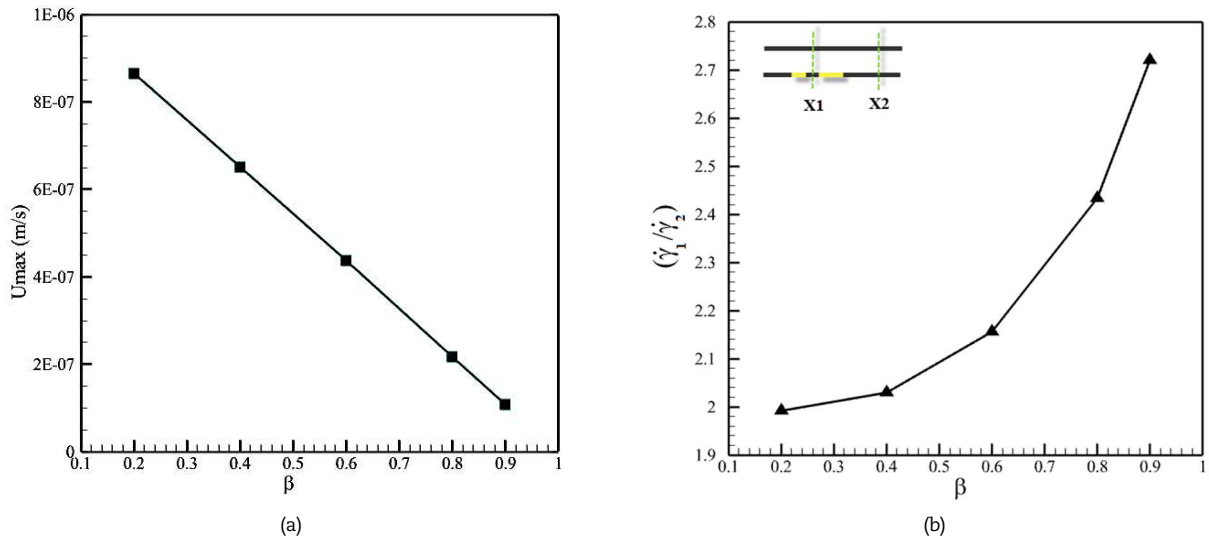
Fig. 6. Effect of the dimensionless number β on (a) the maximum outlet velocity and (b) shear rate ratio.
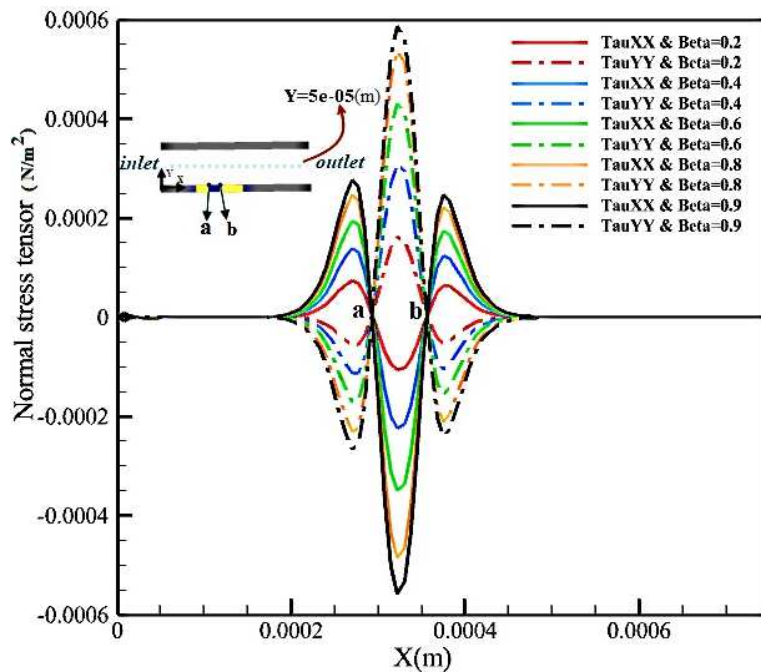
Fig. 7. The β effect on XX and YY normal stress tensors at Y = 5e-05 m.

Figure 7 illustrates the normal stress tensors XX and YY in the longitudinal section Y = 5e-05 m. The normal stress tensors for the X direction are depicted by solid lines, whereas dashed lines show the normal stress tensors for the Y direction. The tensors plotted in the similar β values have the same-colored lines. Distance between the two intermediate nodes (a and b) represents the gap between the pairs of electrodes. In the gap, the impact of the electric field on the fluid flow is much stronger, leading to more pronounced changes in velocity and fluid flow. These significant velocity variations result in an increase in the normal stress tensors in this area, creating different pressure and normal stress variations due to the differences in fluid velocities. For this reason, the magnitude of the normal stress tensors is highest in the region. Thus, the normal stress tensors in the cross-section X = 3.25e-04m, where the maximum stress tensor occurs, will be investigated thoroughly (Figs. 8, 12, 16 and 20). According to [35], the ratio of $(\tau_{xx} - \tau_{yy})$ to τ_{xy} is often considered as a measure of how elastic a fluid is, so the ratio is named as elasticity contours and plots in the present work.

Figure 8-a shows the normal stress tensor at X = 3.25e-04 m of the channel in the X and Y directions. In normal stress tensors, the zero point represents a point in the fluid domain where there is no fluid velocity gradient. Using this definition, the middle node (f) in Figure 8-a represents the point of maximum velocity in the desired section of the fluid domain. Due to the presence of electrodes in the lower wall, the normal stress in the channel between the lower wall and the middle node (f) is greater than the normal stress between the middle node (f) and the upper wall. Normal stress increases as β number increases. There is a very small difference between the magnitude of the normal stress tensors in the distance between the middle nodes (f) and the upper wall of the channel. In Fig. 8-b, the average magnitude of fluid elasticity is shown along the longitudinal axis of the microchannel. Twenty cross-sections through the microchannel are considered in this figure, with the average elasticity of each cross-section calculated separately and displayed as symbols.

(a)

(b)

(c)
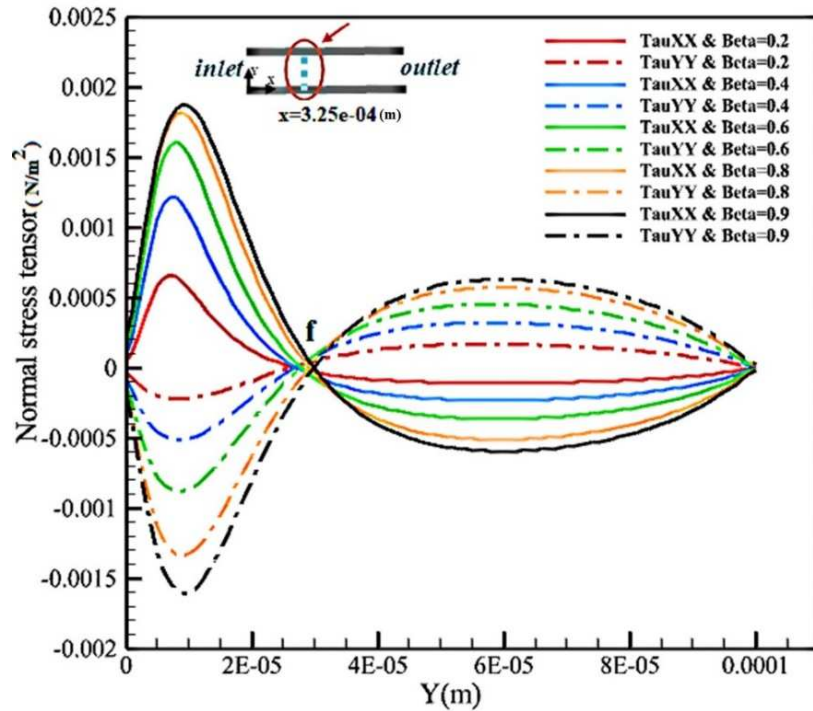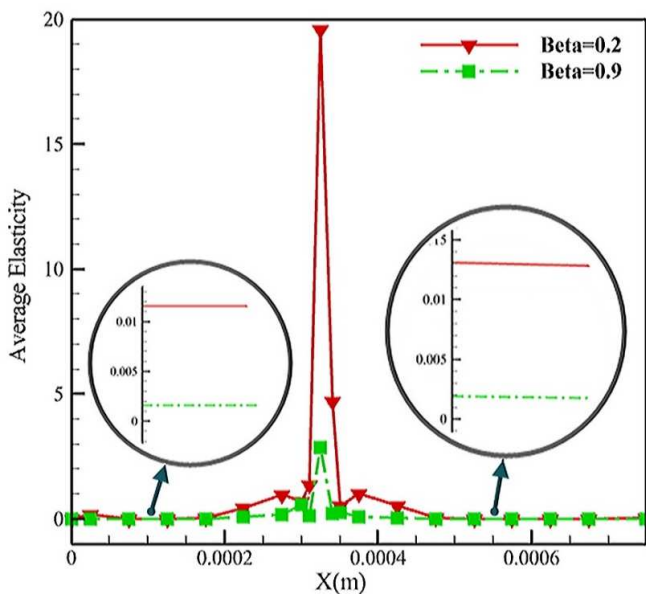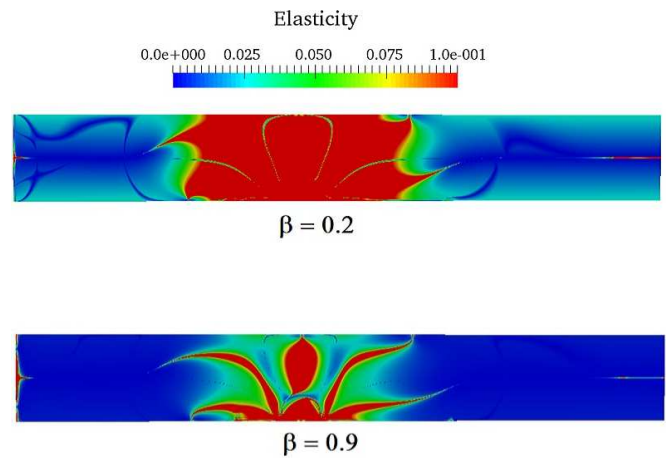
Fig. 8. Effect of β number on (a) XX and YY stress tensors at X = 3.25e-04 m, (b) elasticity magnitude, and (c) elasticity distribution.

The distribution of viscoelastic behavior in the microchannel with β numbers of 0.2 and 0.9 is shown in Fig. 8-c. Since the magnitude of the elasticity is illustrated in Fig. 8-b, the legend number of the contour is limited to 0.1 to better show the viscoelastic behavior distribution. It can be concluded from Figs. 8-b and 8-c that increasing β decreases the elastic behavior of viscoelastic fluid in electrothermal flow which is actually due to the decrease in the velocity and power of electrothermal pumping as a result of the increased viscosity ratio of the polymer to the desired solvent. Figure 8-b shows that the maximum viscoelastic behavior occurs between the electrode gaps, which decreases with the increase in β number.

Figure 9 illustrates the effect of β on the strength of the electrothermal vortices at the 0.2 and 0.6 values of β. According to the figure, the strength of vortices decreases by increasing β.

As shown in Fig. 10, the fluid velocity increases as the Weissenberg number increases. When the Weissenberg number is less than 0.01 and greater than 1, velocity changes are low, whereas when the Weissenberg number is between [0.01, 1], velocity changes are significant. If the Weissenberg number is below 0.01 the behavior of fluid will be more like a Newtonian fluid. When the Wissenberg number becomes larger, the elastic forces resulting from deformation and stresses applied to the fluid become more significant compared to the viscous forces, which are typically associated with a decrease in flow velocity. These interactions lead

to the formation of more complex and stronger vortex structures, which can result in an increase in fluid velocity. Nonetheless, this progression persists only within the limitations set by the geometric capacity of the microchannel. In other hand, according to equation (14), since the Weissenberg number appears as the denominator of the fraction of the second term in the left hand and the first term in the right hand, if the size of the Weissenberg number is large enough or small enough, then the effect of both of these terms or the difference in their effects will decrease, resulting in a decrease in the slope of the velocity curve at both the beginning and end of the plot in Fig. 11-a. As the Weissenberg number increases from 0.001 to 10, the electrothermal outlet velocity increases by 107%. Figure 11-b illustrates that with an increase in the Weissenberg number, the shear rate ratio decreases. Therefore, the transfer of the electrothermal effect from the electrode region to outside the electrode region increases.
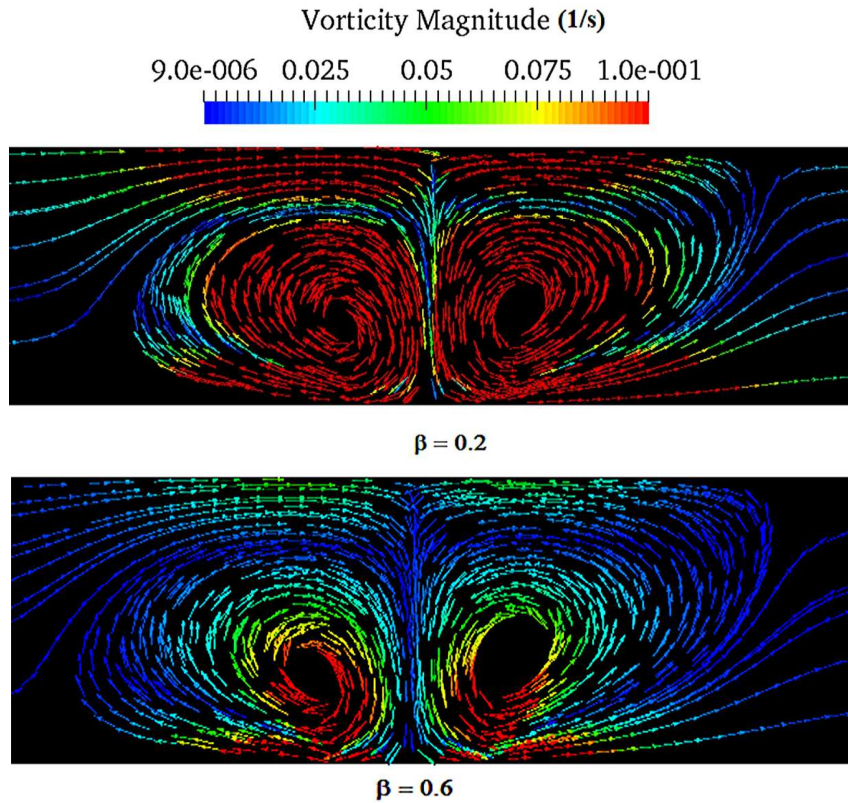
Fig. 9. The effect of a dimensionless β number on the strength of electrothermal flow vortices.
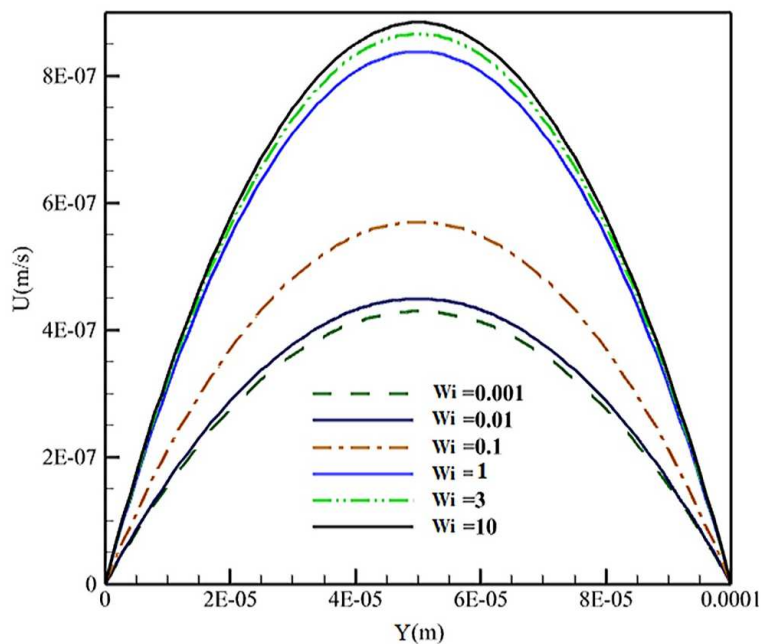
Fig. 10. The effect of the Weissenberg number on electrothermal outlet velocity.

(a)

(b)
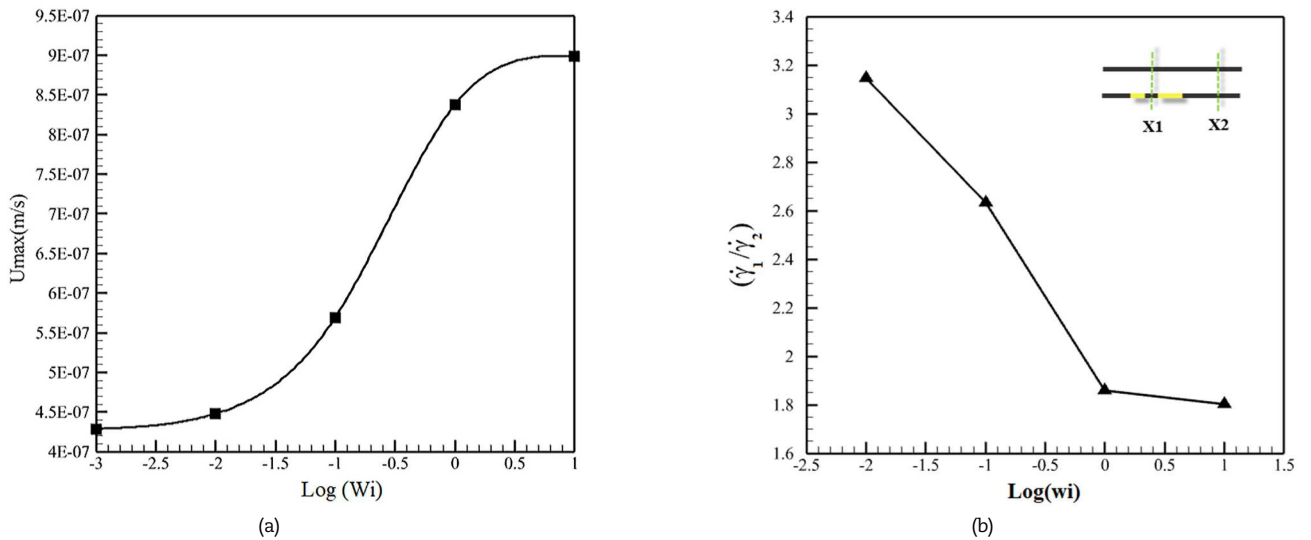
Fig. 11. Effect of Wi number on (a) the maximum outlet velocity and (b) shear rate ratio.
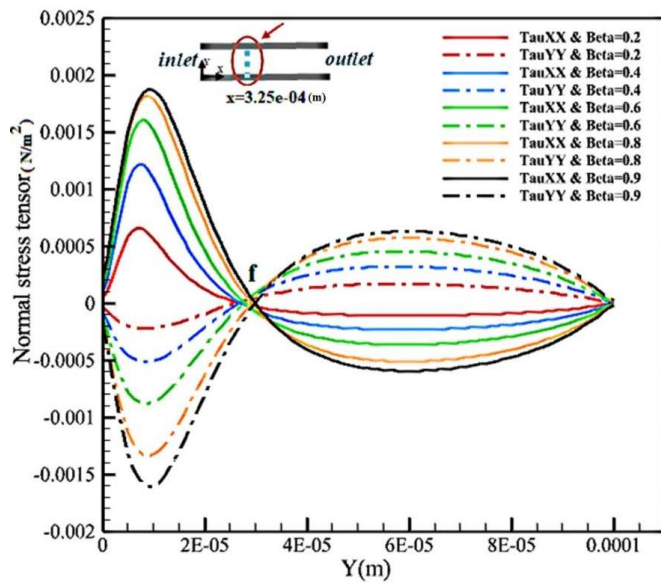
(a)
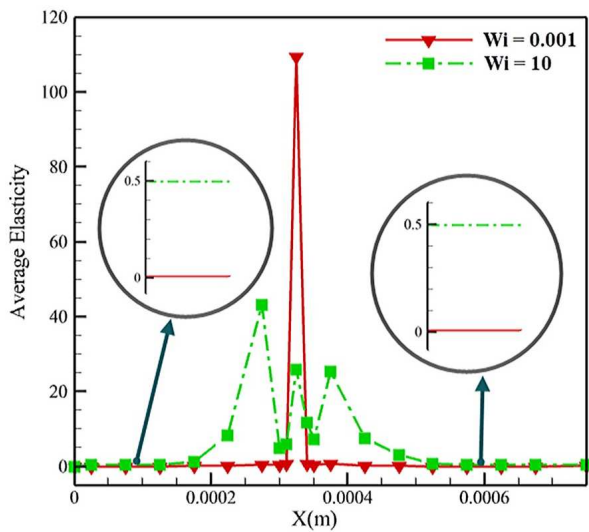
(b)
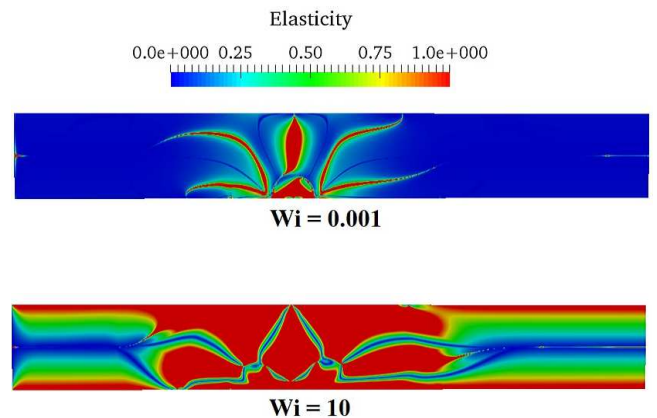
(c)

Fig. 12. The effect of Weissenberg number on (a) X and Y normal stress tensors at X = 3.25e-04 m, (b) elasticity magnitude, and (c) elasticity distribution.

Figure 12-a shows the XX and YY tensors for Weissenberg numbers between 0.001 and 10. Increasing the Weissenberg number increases the effect of viscoelastic force to viscous force so that the normal stress tensors become asymmetric, and the fluid exhibits viscoelastic behavior throughout its domain. A significant effect of Weissenberg on fluid elastic behavior in electrothermal flows is illustrated in Figs. 12-b and 12-c. The behavior occurs so that it spreads from the electrode zone to the walls as Weissenberg increases. In Fig. 12-b, it can be seen that, with increasing Weissenberg number, the magnitude of elasticity in the gap between electrodes decreases, but in other parts of the microchannel, especially on the electrodes zone, the elasticity increases significantly.

Figure 13 illustrates the strength of electrothermal vortices for two Weissenberg numbers of 0.001 and 10. Weissenberg number increases as the ratio of elastic force to viscous force increases, thus decreasing viscous force and increasing the elastic force, leading to an increase in the electrothermal vortices strength of viscoelastic fluids.

An elastic number is a ratio between elastic and inertial force. It has been reported in various works [36, 37], that by increasing this dimensionless parameter, the heat transfer in the fluid domain increases. This parameter is significant in this paper because the electrothermal flow is based on heat transfer and temperature gradients created in the fluid. As shown in Figs. 14 and 15-a, although the elastic number increases the electrothermal velocity in the microchannel, the elastic number effect on outlet velocity is small.
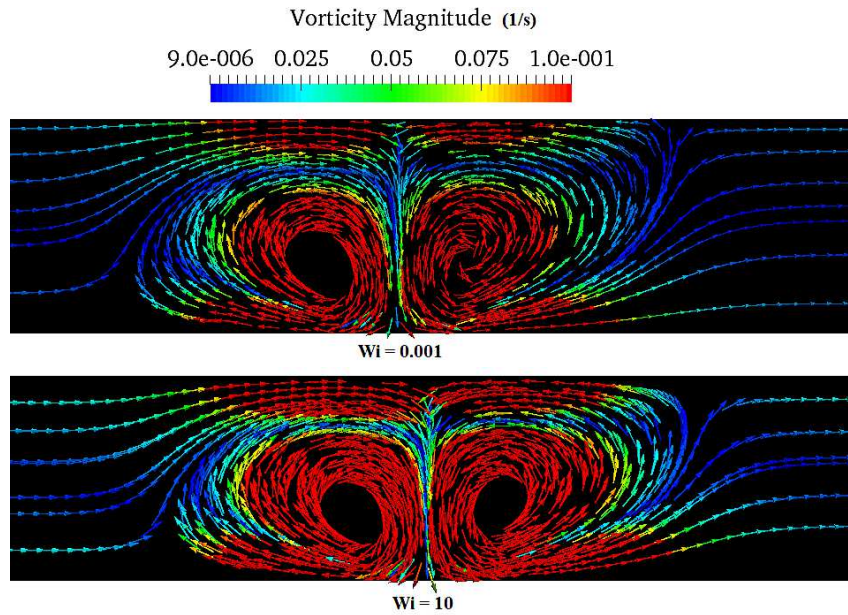
Fig. 13. The effect of Wi number on the strength of electrothermal flow vortices.
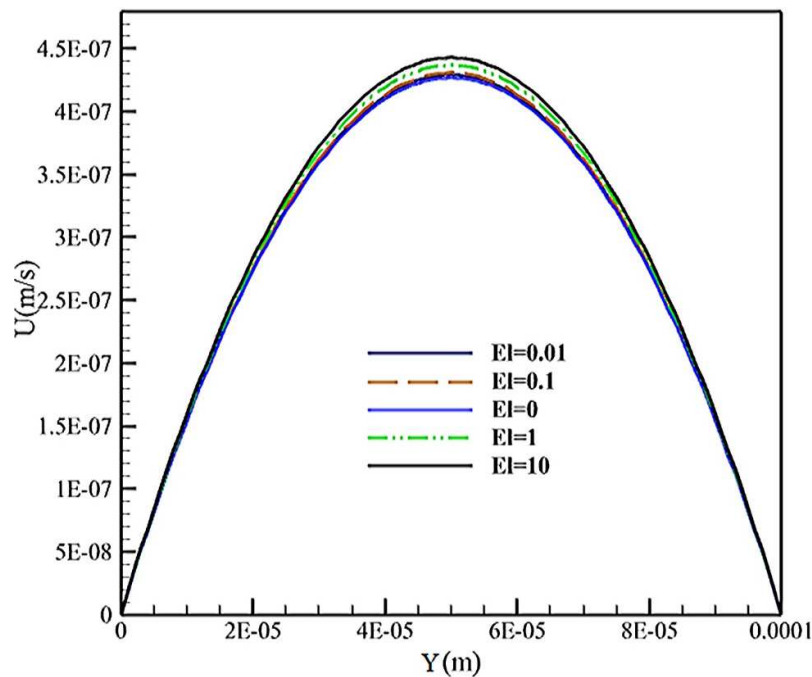
Fig. 14. The effect of the dimensionless elastic number on electrothermal outlet velocity.

(a)

(b)
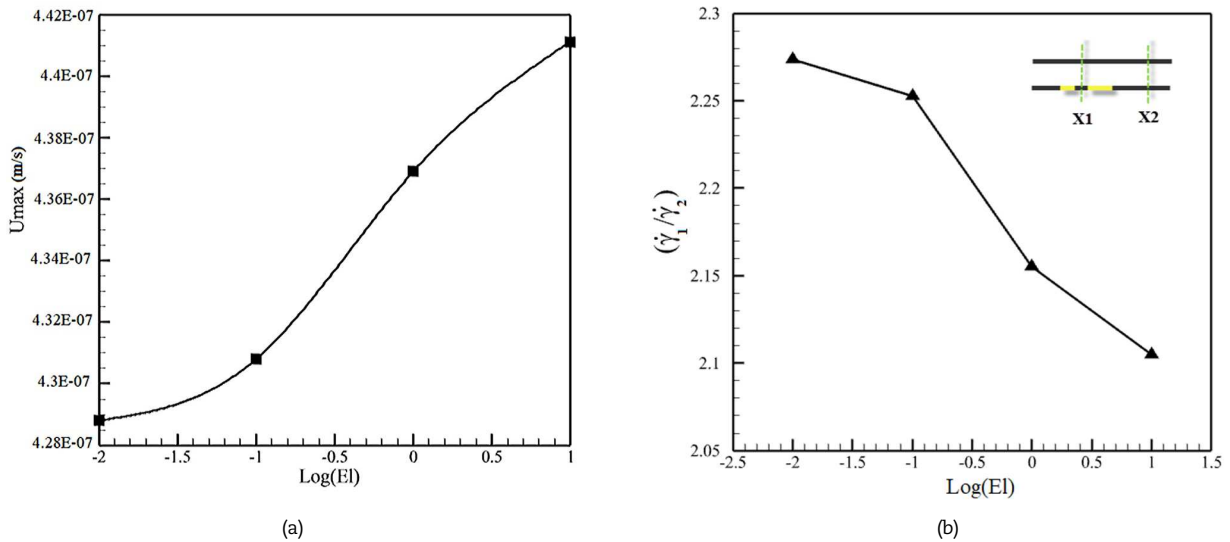
Fig. 15. Effect of the dimensionless El number on (a) the maximum outlet velocity and (b) shear rate ratio.
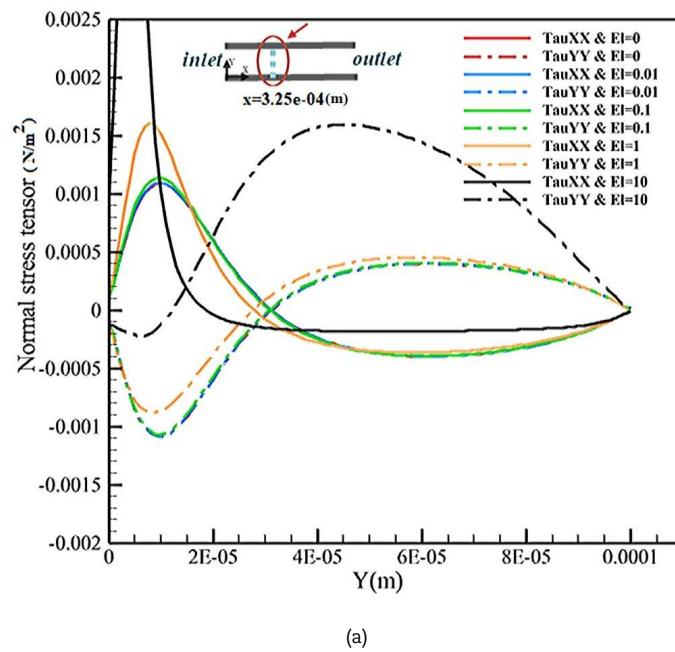
(a)
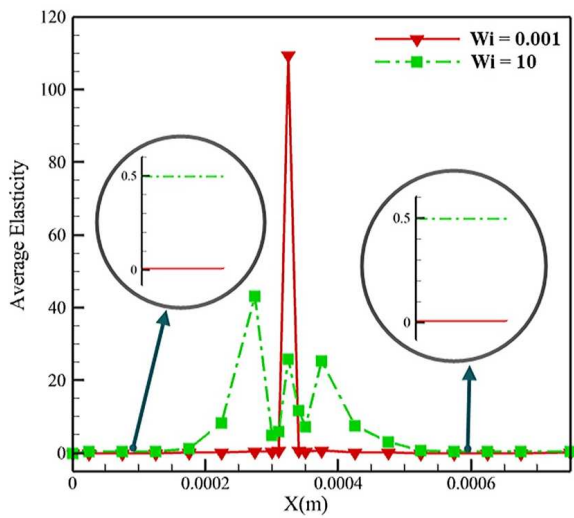
(b)
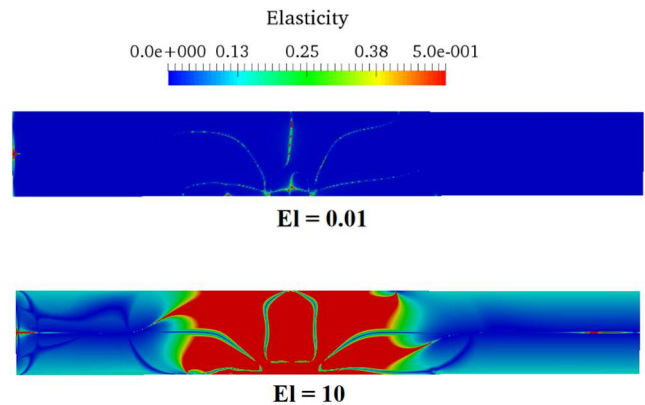
(c)

Fig. 16. The effect of Elastic number on (a) X and Y normal stress tensors at X = 3.25e-04 (m), (b) elasticity magnitude, (c) elasticity distribution.

With an increase in the elastic number, the influence of fluid inertia forces relative to elastic forces actually decreases. Since the Reynolds number range in electrothermal flow is typically low, the effect of inertia forces in this type of flow is also limited and usually manifests itself at higher Reynolds numbers. This factor results in the reduction of the effect of inertia forces on the fluid flow, and the increase in electrothermal flow velocity is primarily due to the increase in elastic forces.

An increase in maximum velocity by increasing the elastic number is shown in Fig. 15-a. As depicted in the figure, the slope of the plot decreases at the beginning and end of the interval. Figure 15-b illustrates the variations in shear rate ratio with changes in elastic number. According to this figure, the variations are most significant for the elastic number range of 0.1 to 1, and with an increase in the elastic number, the shear rate difference ratio decreases.
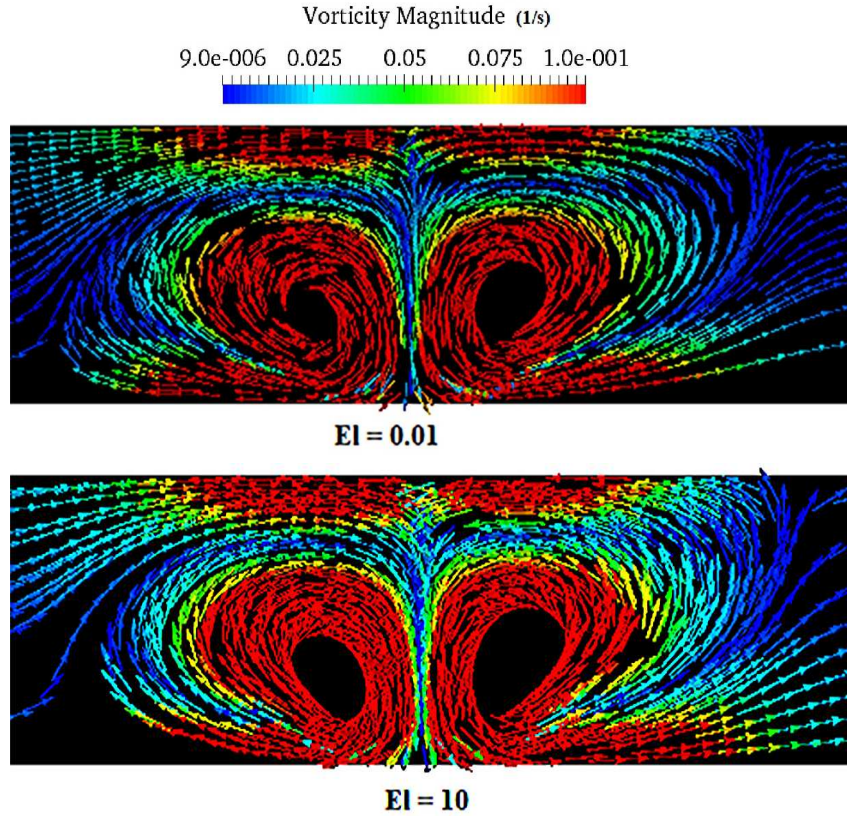
Fig. 17. The effect of a dimensionless El number on the strength of electrothermal flow vortices.
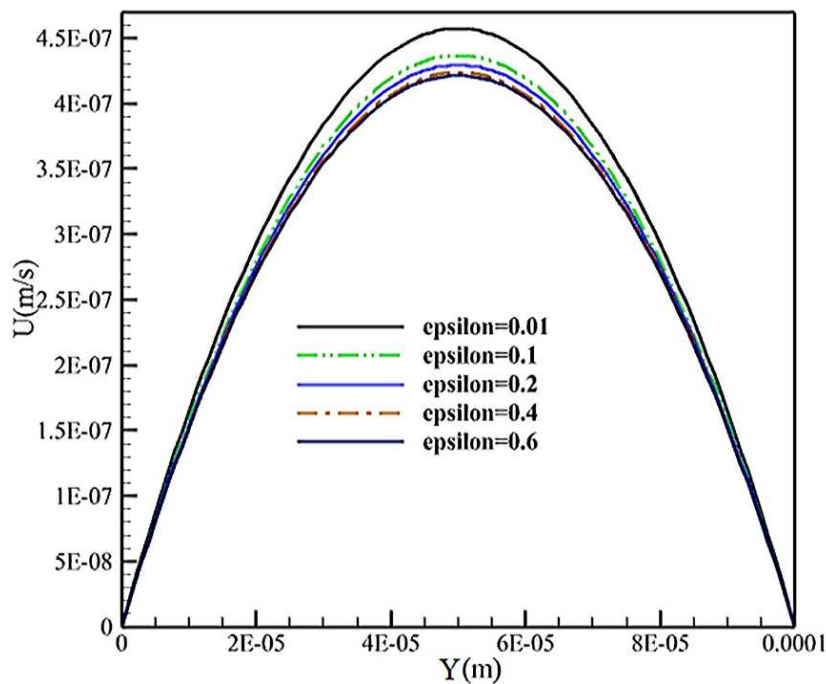
Fig. 18. The effect of the ε number on electrothermal outlet velocity.

Figure 16-a shows the normal stress tensors for different elastic numbers. It has been observed that the difference between the normal stress tensors increases with an increase in elastic number in electrothermal flow. When the elastic number is greater than 1, the place of intersecting normal stress plots gets closer to the channel bottom, and the normal stress tensors are fully asymmetrical throughout the fluid domain. The place of intersecting Normal stress plots gets closer to the channel bottom when the elastic number is greater than 1. The normal stress tensors are fully asymmetrical throughout the fluid domain when the elastic number is more than 1. Figures 16-b and 16-c show that with increasing the elastic number, the viscoelastic behavior of the fluid in the electrothermal flow enhances. Figure 16-b shows the maximum elastic behavior in the gap between electrodes occurs.

Figure 17 illustrates the effect of the elastic number on the strength of vortices in an electrothermal flow. The elastic number is the ratio of elastic to inertial force and increasing this number does not directly affect the velocity gradient. As confirmed in Fig. 17, increasing the elastic number does not significantly affect the strength of the electrothermal vortices.

The PTT model shows a nonlinear behavior for viscoelastic fluids. Using the ε number, one can determine the inherent properties of the fluid, which are inversely proportional to its tensile viscosity [38]. According to Fig. 18, velocity of the fluid decreases with an increase in this parameter. The rate of velocity decline also decreases with the increasing the ε number, Fig. 19-a. Considering Fig. 19-b, the difference in shear rate ratio increases with an increase in the ε number, and the slope of these variations decreases as the ε number increases.

Figure 20-a shows the normal stress tensor variation under the influence of ε number. The elongational viscosity of the material is a measure of its resistance to tensional forces. Since polymer molecule chains are oriented in the flow direction, normal stress tensors follow the same trend as ε changes. As the elastic number increases, normal stress tensors will also increase in magnitude, and simultaneously, the location of maximum velocity moves closer to the electrodes. Normal stress tensors will increase in magnitude when ε is increased. As the ε number increases, the location of maximum velocity becomes closer to the electrodes. According to Figs. 20-b and 20-c, the effect of ε umber on the elastic behavior of viscoelastic fluid in electrothermal flow is insignificant for the range of 0 to 0.8.

(a)   (b)
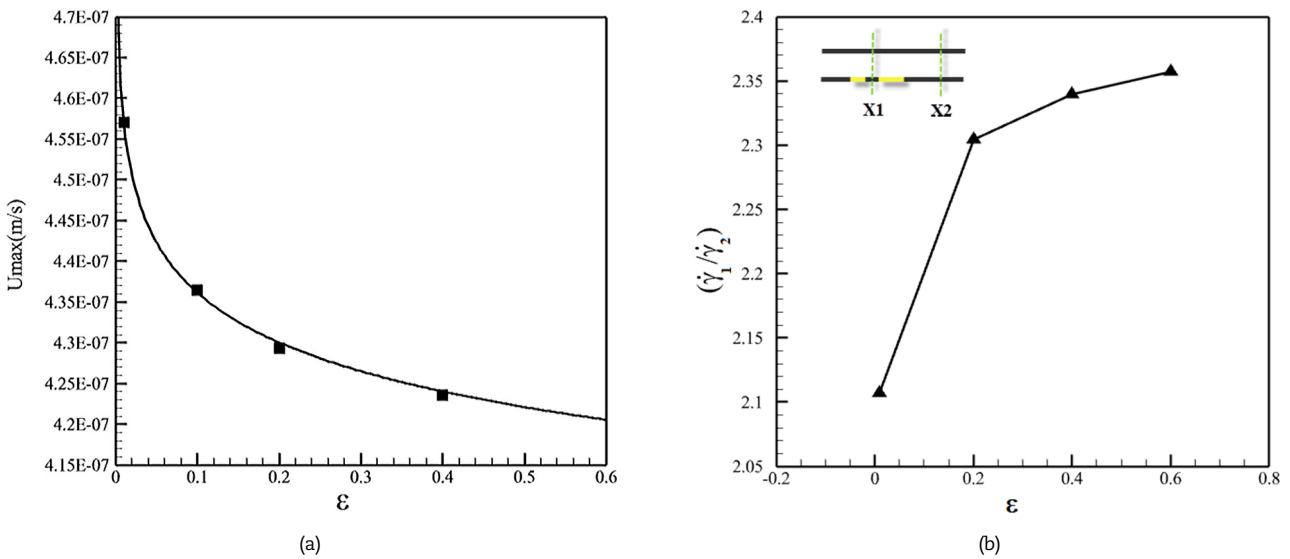
Fig. 19. Effect of the dimensionless ε number on a) the maximum outlet velocity and b) shear rate ratio.

(a)
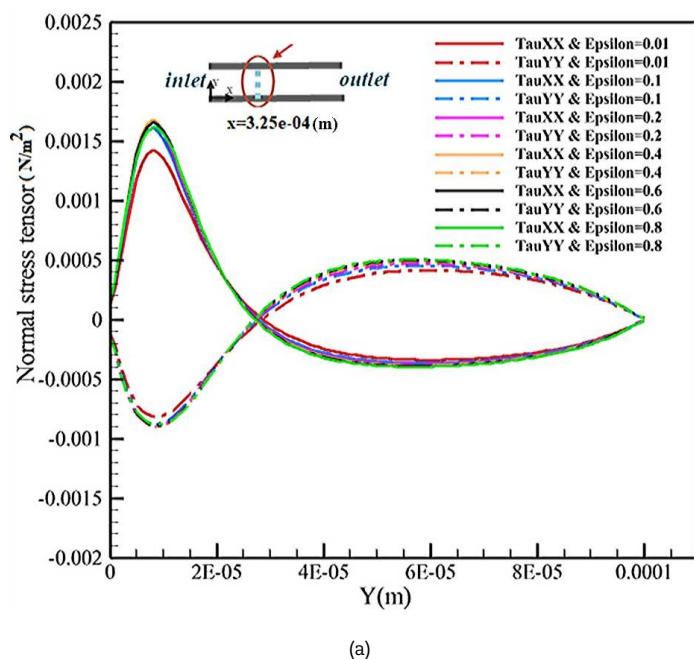
Fig. 20. The ε effect of viscoelastic fluids on (a) X and Y normal stress tensors at X = 3.25e-04 (m), (b) elasticity magnitude, (c) elasticity distribution.

(b)

(c)
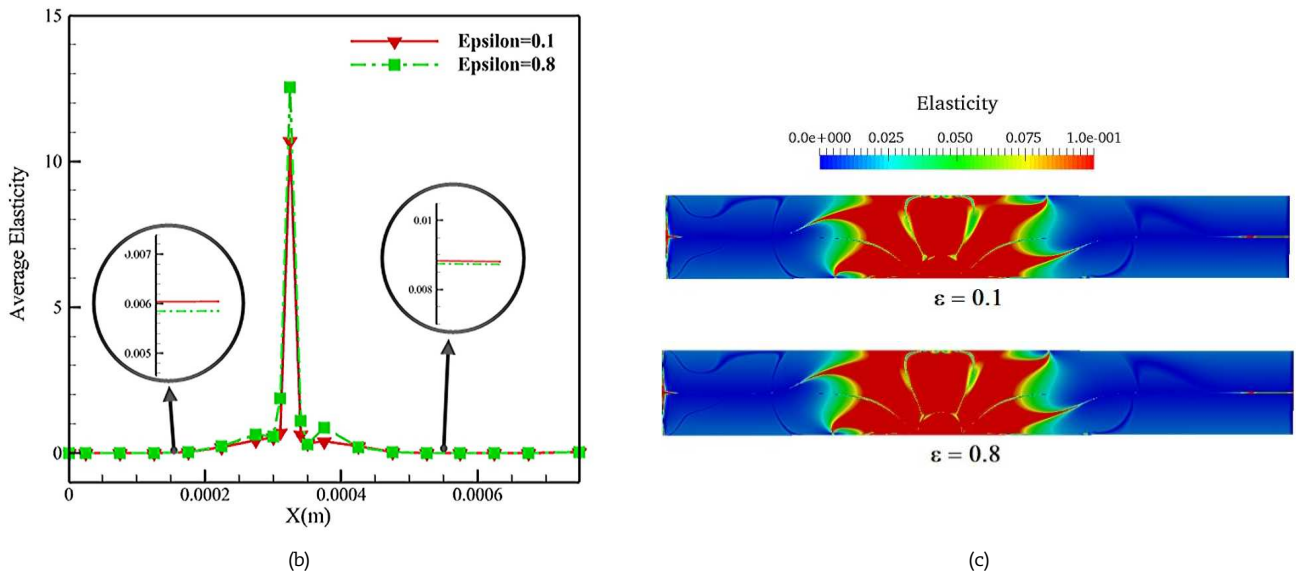
Fig. 20. Continued.
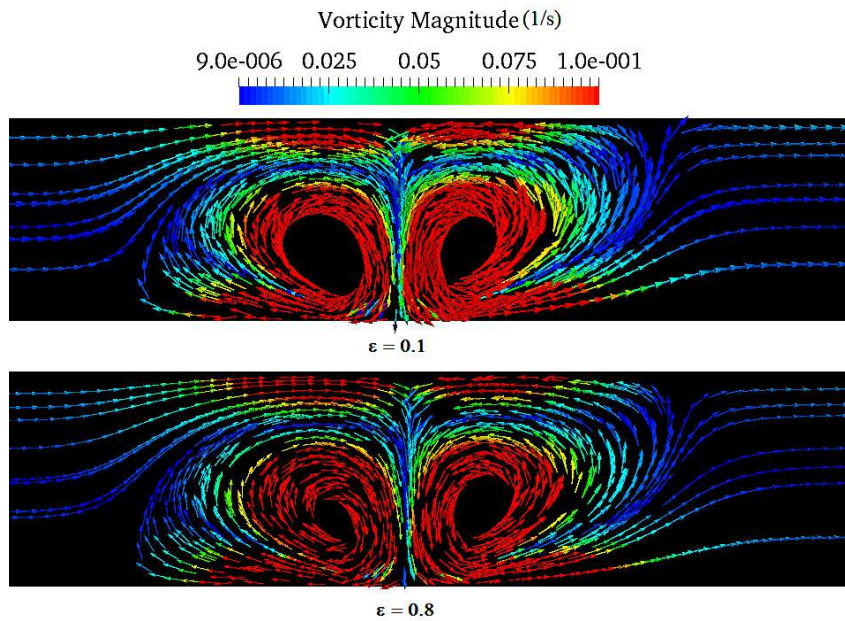
Fig. 21. The effect of a dimensionless ε number on the strength of electrothermal flow vortices.

Figure 21 illustrates the effect of increasing the ε number from 0.1 to 0.8 on the strength of the vortices. Since the shear viscosity primarily determines the shear stress, the variation of the elongation viscosity cannot directly impact the shear stress. However, ε can slightly increase the velocity gradient and the tensor of shear stress, so the effect is not significant on the vortices strength.

Figure 22 shows the effect of viscoelastic dimensionless variables on electrothermal outlet velocity. The effect is accomplished by dividing each maximum velocity by minimum values considering the effect of different viscoelastic dimensionless numbers. The green color indicates a positive effect on velocity increase, while the red color indicates a negative effect. Considering the dimensionless viscoelastic numbers simultaneously inter-effects, Fig. 22 and Eq. (17) indicate sensitivity analyses and show β and Weissenberg numbers significantly affect electrothermal velocity. $\varnothing$ is a hypothetical variable and $S(\varnothing)$ determines the maximum effect of variable $\varnothing$ on electrothermal outlet velocity, expressed in percent. To obtain $S(\varnothing)$, the maximum difference between the outlet velocity created by the variable $\varnothing$, (Umax-Umin), and the minimum outlet velocity created by this variable is divided, and to express it in percentage, it is multiplied by one hundred.

$$S(\beta) = 726\% > S(Wi) = 107\% \; ; \; (\text{higher sensitivity})$$
$$S(\varepsilon) = 8.68\% > S(El) = 2.89\% ; \; (\text{lower sensitivity})$$

(17)

Table 1. Rheological properties of some viscoelastic fluid [29].

Solution	Polymer concentration	λ (ms)	η_0 (mPa.s)
PVP	5%	2.2	28
PEO	3000ppm	2.6	7.9
XG	2000ppm	~0	3680
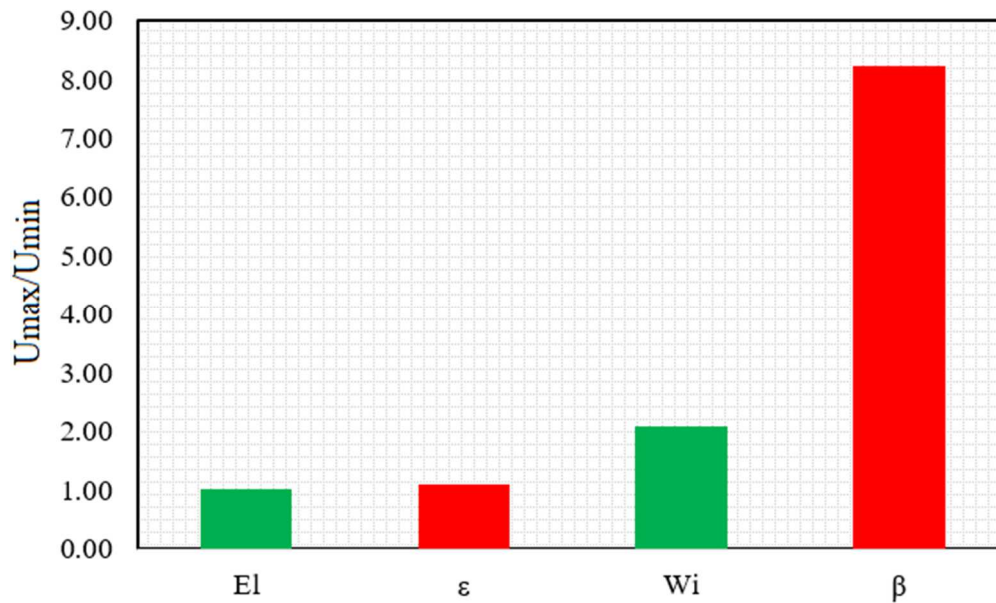
Fig. 22. The effect of different dimensionless viscoelastic variables on electrothermal velocity.

So, viscoelastic fluids with lower viscosity (lower polymer mass fraction when selection is limited to one fluid), and higher relaxation time lead to higher velocity in the electrothermal flow. This fact can be used for choosing the proper type of fluid for a particular purpose; for example, if several viscoelastic fluids can be used for a specific application, the fluid with lower polymer viscosity and longer relaxation time can create a higher velocity in electrothermal flow. According to Table 1, between 5% polyvinylpyrrolidone (PVP) and 3000 ppm polyethylene oxide (PEO) fluids, which are strongly viscoelastic and weakly shear-thinning fluids, and 2000ppm Xuntan gum (XG), which is strongly shear-thinning and weakly viscoelastic, PEO fluid results a higher velocity in electrothermal flow. Another point that can be mentioned is that the velocity can increases by reducing the mass fraction that is important whenever there are limitations in choose of multitype solutions in practical applications.

7. Conclusion

Biological and synthetic polymer solutions with high electrical conductivity are frequently employed in biological applications within the microfluidics field. They are suitable for electrothermal pumping; however, they usually possess viscoelastic properties. Therefore, the main focus of this paper is to investigate the impact of viscoelasticity on electrothermal pumping. To investigate this subject, the effects of the substantial viscoelastic fluid dimensionless numbers, retardation ratio (β), elastic number (El), model parameter (ε), and Weissenberg number (Wi) on the fluid velocity, normal stress tensors, Elasticity behavior, and electrothermal vortices strength were investigated in this study. The results showed that increasing (β) number decreases the electrothermal fluid velocity and elasticity behavior at a constant potential difference. β number reduces electrothermal velocity beyond 700%, associated with a decrease in the strength of the vortices in electrothermal flow. Increasing the Weissenberg number increases velocity and elasticity behavior of viscoelastic fluid in electrothermal flow. The change in velocity with increasing Weissenberg number is non-linear and slightly over 100%. By increasing the Weissenberg number, the region with high elastic behavior of the fluid is extended from the electrode zone to the walls so that the elastic behavior of the fluid is also highly influenced in the range of Wi = 0.001 and 10. As the elastic number increases in the electrothermal flow (in the range of 0.1 to 10), the fluid velocity and elasticity behavior increase. The fluid normal stress tensors, and as a result, the trend of the first normal stress difference completely changes at the elastic number of 10. When the ε number is increased, the velocity of the viscoelastic fluid decreases. The slope of changes in the velocity curve is high at low ε numbers, and decreases with ε. Because of its negligible effect on shear viscosity, the ε number has little effect on Elasticity and vortices strength. According to the simultaneous investigation of different dimensionless variables of viscoelastic fluids, it is evident that viscoelastic fluids with lower viscosity (lower mass fraction of polymer when selection is limited just to one fluid), and higher relaxation time, lead to a higher velocity in the electrothermal flow. So, the type of fluid for a particular purpose can be determined by this fact. As an example, the electrothermal outlet velocity of 3000 ppm PEO solution is higher than 5% PVP and 2000 ppm XG solution.

Author Contributions

The idea of the paper was proposed by A. Ramiar, N. Hedayati developed the solver and conducted the simulations. All authors collaborated in a thorough analysis, result interpretation, and the composition of the discussion section.

Acknowledgments

Not Applicable.

Conflict of Interest

The authors declared no potential conflicts of interest concerning the research, authorship, and publication of this article.

Funding

Data Availability Statements

The datasets generated and/or analyzed during the current study are available from the corresponding author on reasonable request.

Nomenclature

Br	Brinkman number	ε_m	Electrical Permittivity (C/V.m)
C_p	Fluid specific heat capacity (J/kg.°C)	σ_m	Electrical conductivity (S/m)
H	Channel height	Pe	Peclet number
El	Elastic number	ρ_q	Electric charge density (C/m³)
E_0	Electrical field (V)	ρ	Fluid density (kg/m³)
f	PTT model function	ξ	Slip parameter
F_{ET}	Electrothermal force (N/m³)	β	Retardation ratio
k	Thermal conductivity (W/K.m)	λ	Relaxation time (s)
Pr	Prantel number	ε	Model parameter
P	Pressure (Pa)		**Index**
Pe	Peclet number	w	Wall
Re	Reynolds number	m	Medium
t	Time (s)	·	Total
T	Temperature (K)	s	Solvent
U	Fluid velocity (m/s)	p	Polymer
Wi	Weissenberg number	in	Inlet
	Greek symbols		**Superscripts**
γ	Deformation rate tensor	*	Non-dimensionalized
τ	Stress tensor (Pa)	p	Polymer
φ	Electrical potential (V)	s	Solvent
$\varnothing$	Hypothetical variable		
η	Viscosity (N.s/m²)		

References

[1] Salari, A., Navi, M., Lijnse, T., Dalton, C., AC electrothermal effect in microfluidics: A review, *Micromachines*, 10(11), 2019, 762.

[2] Alipanah, M., Hafttananian, M., Hedayati, N., Ramiar, A., Alipanah, M., Microfluidic on-demand particle separation using induced charged electroosmotic flow and magnetic field, *Journal of Magnetism and Magnetic Materials*, 537, 2021, 168156.

[3] Ghasemi, A., Ramiar, A., Numerical investigation of continuous acoustic particle separation using electrothermal pumping in a point of care microfluidic device, *Chemical Engineering and Processing-Process Intensification*, 176, 2022, 108964.

[4] Ramos, A., Morgan, H., Green, N.G0, Castellanos, A. Ac electrokinetics: a review of forces in microelectrode structures, *Journal of Physics D: Applied Physics*, 31(18), 1998, 2338.

[5] Green, N.G., Ramos, A., González, A., Castellanos, A., Morgan, H., Electric field induced fluid flow on microelectrodes: the effect of illumination, *Journal of Physics D: Applied Physics*, 33(2), 2000, L13.

[6] Sigurdson, M., Wang, D., Meinhart, C.D., Electrothermal stirring for heterogeneous immunoassays, *Lab on a Chip*, 5(12), 2005, 1366-73.

[7] González, A., Ramos, A., Morgan, H., Green, N.G., Castellanos, A., Electrothermal flows generated by alternating and rotating electric fields in microsystems, *Journal of Fluid Mechanics*, 564, 2006, 415-33.

[8] Wu, J., Lian, M., Yang, K., Micropumping of biofluids by alternating current electrothermal effects, *Applied Physics Letters*, 90(23), 2007, 234103.

[9] Du, E., Manoochehri, S., Enhanced ac electrothermal fluidic pumping in microgrooved channels, *Journal of Applied Physics*, 104(6), 2008, 064902.

[10] Du, E., Manoochehri, S., Microgrooves Enhanced AC Electrothermal Pumping for High Conductivity Microfluids, *ASME 2008 International Design Engineering Technical Conferences and Computers and Information in Engineering Conference,* American Society of Mechanical Engineers, 2008.

[11] Yang, K., Wu, J., Investigation of microflow reversal by ac electrokinetics in orthogonal electrodes for micropump design, *Biomicrofluidics*, 2(2), 2008, 024101.

[12] Lian, M., Wu, J., Microfluidic flow reversal at low frequency by AC electrothermal effect, *Microfluidics and Nanofluidics*, 7(6), 2009, 757.

[13] Sin, M.L., Gau, V., Liao, J.C., Wong, P.K., Electrothermal fluid manipulation of high-conductivity samples for laboratory automation applications, *Journal of the Association for Laboratory Automation*, 15(6), 2010, 426-32.

[14] Du, E., Manoochehri, S., Microfluidic pumping optimization in microgrooved channels with ac electrothermal actuations, *Applied Physics Letters*, 96(3), 2010, 034102.

[15] Zhang, R., Dalton, C., Jullien, G.A., Two-phase AC electrothermal fluidic pumping in a coplanar asymmetric electrode array, *Microfluidics and Nnanofluidics*, 10(3), 2011, 521-9.

[16] Hong, F., Bai, F., Cheng, P., Numerical simulation of AC electrothermal micropump using a fully coupled model, *Microfluidics and Nanofluidics*, 13(3), 2012, 411-20.

[17] Zhang, R., Jullien, G.A., Dalton, C., Study on an alternating current electrothermal micropump for microneedle-based fluid delivery systems, *Journal of Applied Physics*, 114(2), 2013, 024701.

[18] Williams, S.J., Enhanced electrothermal pumping with thin film resistive heaters, *Electrophoresis*, 34(9-10), 2013, 1400-8.

[19] Stubbe, M., Gyurova, A., Gimsa, J., Experimental verification of an equivalent circuit for the characterization of electrothermal micropumps: High pumping velocities induced by the external inductance at driving voltages below 5 V, *Electrophoresis*, 34(4), 2013, 562-74.

[20] Salari, A., Navi, M., Dalton, C., AC electrothermal micropump for biofluidic applications using numerous microelectrode pairs, *2014 IEEE Conference on Electrical Insulation and Dielectric Phenomena (CEIDP)*, IEEE, 2014.

[21] Salari, A., Dalton, C., A novel AC electrothermal micropump for biofluid transport using circular interdigitated microelectrode array. Microfluidics, *BioMEMS, and Medical Microsystems XIII*, International Society for Optics and Photonics, 2015.
[22] Williams, S.J., Green, N.G., Electrothermal pumping with interdigitated electrodes and resistive heaters, *Electrophoresis*, 36(15), 2015, 1681-9.
[23] Vafaie, R.H., Ghavifekr, H.B., Configurable ACET micro-manipulator for high conductive mediums by using a novel electrode engineering, *Microsystem Technologies*, 23(5), 2017, 1393-403.
[24] Hong, F., Cao, J., Cheng, P., A parametric study of AC electrothermal flow in microchannels with asymmetrical interdigitated electrodes, *International Communications in Heat and Mass Transfer*, 38(3), 2011, 275-9.
[25] Kunti, G., Bhattacharya, A., Chakraborty S. Analysis of micromixing of non-Newtonian fluids driven by alternating current electrothermal flow, *Journal of Non-Newtonian Fluid Mechanics*, 247, 2017, 123-31.
[26] Shojaei, A., Ramiar, A., Ghasemi, A.H., Numerical investigation of the effect of the electrodes bed on the electrothermally induced fluid flow velocity inside a microchannel, *International Journal of Mechanical Sciences*, 157, 2019, 415-27.
[27] Park, H., Lee, W., Effect of viscoelasticity on the flow pattern and the volumetric flow rate in electroosmotic flows through a microchannel, *Lab on a Chip*, 8(7), 2008, 1163-70.
[28] Huang, Y., Chen, J., Wong, T., Liow, J.L., Experimental and theoretical investigations of non-Newtonian electro-osmotic driven flow in rectangular microchannels, *Soft Matter*, 12(29), 2016, 6206-13.
[29] Ko, C.H., Li, D., Malekanfard, A., Wang, Y.N., Fu, L.M., Xuan, X., Electroosmotic flow of non-Newtonian fluids in a constriction microchannel, *Electrophoresis*, 40(10), 2019, 1387-94.
[30] Ji, J., Qian, S., Liu, Z., Electroosmotic flow of viscoelastic fluid through a constriction microchannel, *Micromachines*, 12(4), 2021, 417.
[31] Sibley, D.N., *Viscoelastic flows of PTT fluids*, University of Bath, UK, 2010.
[32] Spagnolie, S.E., Complex fluids in biological systems. Biological and Medical Physics, *Biomedical Engineering*, 2015.
[33] Minaeian, A., Nili-Ahmadabadi, M., Norouzi, M., Forced convective heat transfer of nonlinear viscoelastic flows over a circular cylinder at low Reynolds inertia regime, *Communications in Nonlinear Science and Numerical Simulation*, 83, 2020, 105134.
[34] Vafaie, R.H., Ghavifekr, H.B., Van Lintel, H., Brugger, J., Renaud, P., Bi-directional ACET micropump for on-chip biological applications, *Electrophoresis*, 37(5-6), 2016, 719-26.
[35] Gan, H.Y., Lam, Y.C., *Viscoelasticity*, In: Encyclopedia of Microfluidics and Nanofluidics, Boston, Springer USA, 2013.
[36] Pinho, F., Coelho, P., Fully-developed heat transfer in annuli for viscoelastic fluids with viscous dissipation, *Journal of Non-newtonian Fluid Mechanics*, 138(1), 2008, 7-21.
[37] Mahdavi Khatibi, A., Mirzazadeh, M., Rashidi, F., Forced convection heat transfer of Giesekus viscoelastic fluid in pipes and channels, *Heat and Mass Transfer*, 46(4), 2010, 405-12.
[38] Ferrás, L.L., Nóbrega, J.M., Pinho, F.T., Analytical solutions for channel flows of Phan-Thien–Tanner and Giesekus fluids under slip, *Journal of Non-Newtonian Fluid Mechanics*, 171, 2012, 97-105.

ORCID iD

Nima Hedayati [iD] https://orcid.org/0000-0003-0314-2162
Abas Ramiar [iD] https://orcid.org/0000-0003-0777-2778
Kurosh Sedighi [iD] https://orcid.org/0000-0001-9549-9382

Publisher's Note Shahid Chamran University of Ahvaz remains neutral with regard to jurisdictional claims in published maps and institutional affiliations.